Edinburgh Research Explorer

Characterization of mode I interlaminar properties of novel composites for tidal turbine blades

Characterization of mode I interlaminar properties of novel composites for tidal turbine blades

Christophe Floreani, Colin Robert, Parvez Alam, Peter Davies and Conchúr M. Ó Brádaigh

Abstract—Tidal turbine blades are exposed to very high loads and are shorter than wind turbine blades requiring thicker composite sections making manufacturing a slow process. However, powder epoxy, which has a low viscosity and a low exothermic reaction, is suitable for rapid out-of-autoclave manufacturing of large composite structures such as turbine blades. In this paper, we describe a process that has been developed to manufacture powder epoxy based carbon and glass fibre reinforced plastic (CFRP and GFRP, respectively) laminates. Through thickness measurements, resin burn-off and microscope observations, the process was shown to be reliable and to produce consistent parts. The in-plane mechanical properties were measured through tensile testing and low scatter was observed in the GFRP coupons as compared to the CFRP coupons. Difficulties experienced in maintaining uniform alignment of the carbon fibre bundles explains the higher scatter obtained on the longitudinal tensile strength. The mode I interlaminar fracture toughness was obtained for the CFRP samples with a G_{IC} of 1.92 kJ/m^2. It was found to be substantially higher than values reported in literature for carbon/epoxy prepreg systems, making it suitable for use in areas of a tidal turbine blades exposed to high stresses such as near ply drops where the risk of delamination is enhanced.

Index Terms—Fracture Mechanics, Composites Manufacturing, Mechanical Characterisation, Tidal Turbine Blades

I. INTRODUCTION

DEPLETION of fossil fuels as well as a sharp increase in atmospheric CO2 concentrations, have led to an increased spending in R&D on sustainable energy sources in recent decades. If this has led to a rapid development and deployment of wind and solar energies, ocean energy remains a largely untapped source. With an estimated 8000 TWh/year [1] of technically recoverable energy, mostly in the form of wave and tidal energy, and an estimated total capacity of 100-200 GW by 2050 [2], ocean energy has the potential to play an active role in a future sustainable energy grid. Also, as the behaviour of tides is well known [3], tidal energy is a highly predictable source of energy which means it can serve as base load [4], making it more valuable than intermittent sources of renewable energy such as wind and solar power.

C. Floreani, C. Robert, P. Alam and C. M. Ó Brádaigh are in Institute for Materials and Processes at the School of Engineering of the University of Edinburgh,Robert Stevenson Road, King's Buildings, Edinburgh EH9 3FB (e-mail: christophe.floreani@ed.ac.uk, colin.robert@ed.ac.uk, parvez.alam@ed.ac.uk, c.obradaigh@ed.ac.uk).

P. Davies is at the French Research Institute for Exploitation of the Sea (IFREMER) Centre de Bretagne, Marine Structures Laboratory, 29280 Plouzan, France (e-mail: peter.davies@ifremer.fr).

However, recent development of the tidal energy market have been hindered by very high costs with a Levelized Cost of Energy (LCOE) of £170/MWh [5], which means that, at present, tidal energy cannot compete against either fossil fuels or other forms of renewable energy. Uncertainties in material properties, manufacturing variability, and the lack of accurate models for the prediction of loads on tidal turbine blades [6] have led to overly conservative designs that are not cost effective.

Tidal turbine blades account for 10-15 % [7], [8] of the cost of a tidal turbine project and can lead to a significant increase in the operational and maintenance costs if they fail prematurely. Much like wind turbine blades, their large size makes them unsuitable for autoclave manufacturing and they are usually built using vacuum infusion, vacuum assisted resin transfer moulding (VARTM) or using out-of-autoclave prepregs. However, there are design differences between blades used in the wind and tidal energy industries, which leads to further difficulties in scaling up the production of high quality tidal turbine blades. As the density of water is 800 times that of air, the forces generated on a tidal turbine blade are comparatively much higher than for wind turbines. This leads to tidal blades being much shorter than equivalent rated wind turbines, with a typical rotor diameter of around 20m for a 1.5 MW turbine [9], despite being exposed to similar bending moments. These blades are therefore stiffer and stronger than their wind industry counterparts, and thicker blades are consequently required.

The rapid manufacturing of thick composites leads to difficulties for two main reason. First, the thermal conductivity of the resin and glass fibres is low, leading to thermal gradients and a lower degree of cure at the core of the laminate. Second, the exothermic reaction of the resin leads to a high thermal peak being reached in the centre of the laminate, with the potential for overcuring in the system leading to detrimental mechanical properties [10]. Recent research on blade manufacturing has led to the development of a novel process using heated tooling and powder epoxy [7], [11]. The powder epoxy resin produces a very low exothermic reaction with an enthalpy of 140 to 180 J/g compared to 300 to 500 J/g for conventional epoxy resins [12], allowing for speedier curing of thick laminates. This resin has also a good thermal stability, allowing it to be stored at room temperature for several years. It also has a low viscosity [12] enabling the manufacturing of parts with low porosity. Another interesting feature of this

powder epoxy is that it melts between 45°C and 100°C [12] without leading to a significant degree of cure, allowing blade halves to be formed separately and co-cured in a one shot process without requiring the use of adhesives [11].

As tidal blades are short compared to wind blades, there is a much more rapid transition from a circular root section to the first hydrofoil leading to high curvatures and out of plane stresses [13]. This leads to ply drops occurring over a short distance along the blade, especially near the root [14]. These areas of high stress increase the likelihood of crack initiation and propagation along interfaces between plies [15]. Quantifying the interlaminar fracture toughness of the composite used in the manufacturing process is therefore of considerable importance in the design of higher fracture resistant composites.

This paper describes how a process was developed for the manufacturing of flat carbon fibre and glass fibre powder epoxy plates and was shown to be reliable and to produce consistent parts. The in-plane mechanical properties and mode I interlaminar fracture toughness properties of these powder epoxy GFRP and CFRP composites were then measured through mechanical testing.

II. EXPERIMENTAL PROCEDURE

A. Materials

Fabrics which are readily available in the market are more likely to be suitable for the manufacturing of tidal turbine blades in the near future than specialised fabrics often studied in research projects. This is why fabrics were purchased from SAERTEX ®. The fracture behaviour of woven or multi-directional composites is more complicated than in unidirectional (UD) materials, with unstable crack growth following the woven pattern and hence deviating from single mode delamination [16]. It was therefore decided to work with UD fabrics, which are also commonly used in the tidal industry, as a first step towards characterising the interlaminar fracture toughness properties of fibre reinforced powder epoxy composites. A further objective was to investigate and quantify potential differences in the behaviour of powder epoxy GFRP and CFRP. Hence, the following two fabrics were studied: (i) a UD stitched carbon fabric (U-C-603 g/m^2-1230 mm) with 581 g/m^2 Zoltek Panex 35-13 50K 0° fibres, 16g/m^2 ±60° E-glass fibres and 6g/m^2 polyester stitching [17]; and (ii) a UD stitched glass fabric (U-E-591 g/m^2-1200 mm) with 520 g/m^2 E-glass 1.200 TEX fibres, 54 g/m^2 90° E-glass fibres and 17 g/m^2 polyester stitching [18].

B. Manufacturing Procedure

As powder epoxy possesses a low minimum viscosity (prior to gelation), it has a tendency to bleed out from the composite during the curing stage, which can lead to a high variation in the fibre volume fraction (FVF) of the final parts. It furthermore makes it difficult to manufacture plates at a specific FVF. As a means of remediating this, a manufacturing process was developed as part of this work. A frame with inner dimensions of 300 mm x 280 mm was manufactured as shown in Fig. 1, from an 8 mm thick stainless steel plate. Two stainless steel caul plates were used in the process with the top one designed have a tight fit into the frame, ensuring that uniform pressure was exerted by the applied vacuum, as well as limiting the resin bleed-out. To allow for easy removal of the plates, the caul plates were covered in TFG 250 PTFE coated glass fibre and thin TF 050AH PTFE tape was applied on the frame. Powder epoxy was sprinkled evenly before the first ply and subsequently between each ply. The weight of powder epoxy was calculated using the resin and fabric densities to lead to a 50% FVF for the finished plates, and was evenly distributed distributed between the plies. This process ensured a good fibre wetting and an even resin distribution. Once the layup was complete, the system was vacuum bagged and cured in an oven.

C. Curing Cycle

As the resin was stored in the laboratory at room temperature for several months, it was susceptible to absorbing humidity. Therefore, the first step of the curing cycle involved drying by exposing the laminate to 55°C temperature environment for eight hours. This stage also lowers the viscosity of the resin as it starts to sinter and melt around this temperature allowing for fibre impregnation. This is followed by two hours of curing at 135°C, followed by two hours of post-cure at 185°C.

D. Testing Methods

The tensile tests were performed according to BS EN ISO 527 using 0°, 90° and ±45° coupons. The samples were machined using a Benetec® diamond coated wet saw to a length of 250 mm and a width of 25 mm. The plates used for this test were 4 plies thick, leading to an average plate thickness of 1.79 mm and 2.30 mm for the GFRP and CFRP plates respectively. 5 coupons were extracted for each test as required by the standard. The test was performed using an MTS Criterion C45 Universal Test Machine using a crosshead displacement of 2mm/min and a 300kN load cell. Glass fibre end-tabs were bonded on to the specimens to limit local stress concentrations at the grips of the MTS machine. Paint was speckled on the coupons to allow for strain measurement with an Imetrum Video Extensometer. The stiffness and Poisson's ratio were measured from a strain of 0.05 % to 0.25 %. The shear modulus was calculated from the ±45° samples using Equation 1:

$$G_{12} = \frac{E_x}{2(1 + v_{xy})} \quad (1)$$

Where E$_x$ is the tensile modulus of the ±45° coupons and v$_{xy}$ is the Poisson's ratio both measured in the x-direction which is the direction of crosshead displacement.

A Double Cantilever Beam (DCB) test was conducted on the CFRP samples following ASTM D5528-13. This allowed the measurement of the critical mode I strain
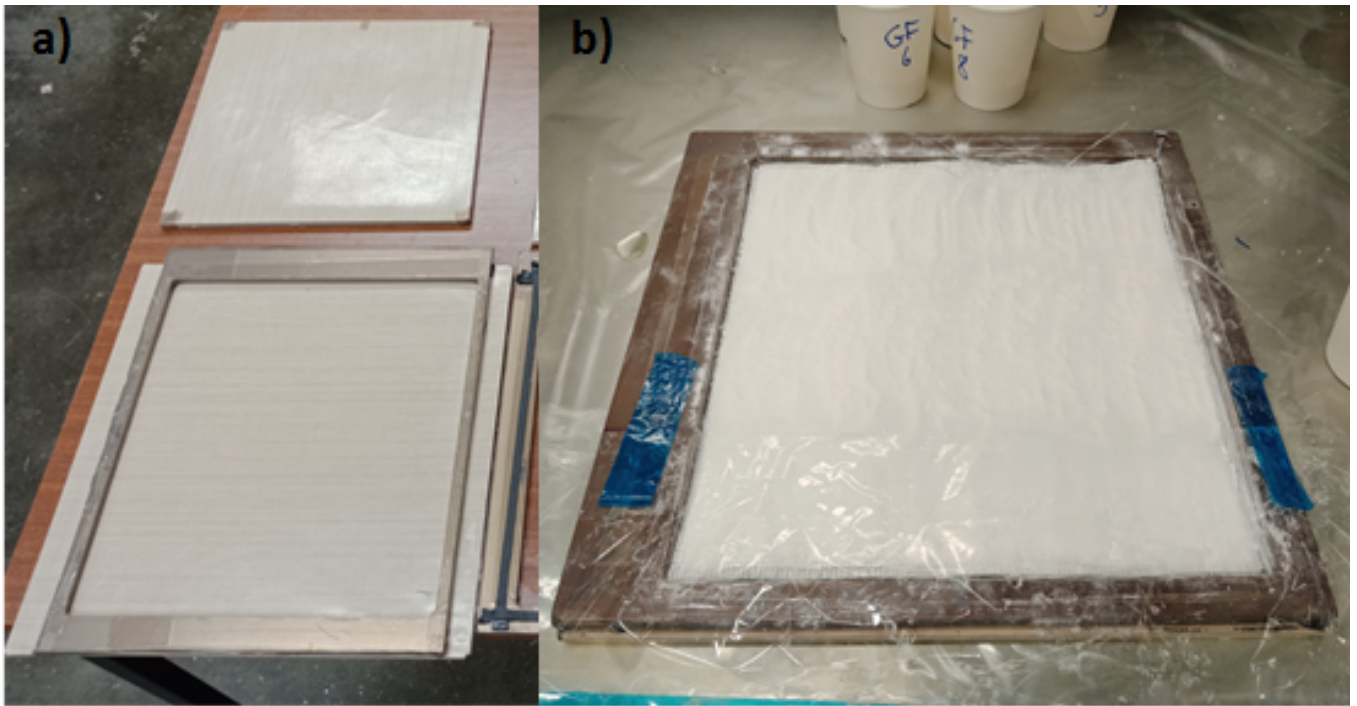
Fig. 1. Frame Designed for Manufacturing Fibre Reinforced Epoxy Plates a) before layup b) during DCB plate manufacturing.

Fig. 2. Specimen Manufactured for Double Cantilever Beam Testing with Speckling Pattern.

TABLE I
THICKNESS MEASUREMENTS OF THE COMPOSITE PLATES

Materials	Number of Plies	Average Thickness (mm)	Standard Deviation (mm)
Carbon Fibre	4	2.31	0.019
	6	3.46	0.085
Glass Fibre	4	1.79	0.0024
	6	2.64	0.016
	8	3.49	0.019

energy release rate per unit area during crack propagation, (G_{IC}). The test was conducted on a 3369 series Instron 50 kN Universal Test Machine equipped with a 1kN load cell. Stainless steel loading blocks were bonded to the ends of the composite using VTFA 400 adhesive and a constant crosshead displacement of 1 mm/min was used. The plates were manufactured with 6 plies giving an average specimen thickness of 3.49 mm. A 13-μm thick PTFE film was inserted in the middle of the plate with a length of 60 mm as shown in Fig. 1 b). In order to track the crack propagation, white paint was applied to the side of the specimen as seen in Fig. 2. A random pattern of black dots were then drawn on the white paint, allowing the Manta G-146B/G-146C camera and the Imetrum video extensometer to record the crack extension in real time.

III. INSPECTION OF MANUFACTURING QUALITY

E. Thickness Distribution

To investigate the presence of defects or resin rich regions, the thickness of each plate tested was measured at 12 different points using a Kroeplin® thickness gauge. Table I summarises the results of the thickness measurements. For the CFRP plates, four 6-ply as well as three 4-ply plates were measured, while four 8-ply, four 6-ply and three 4-ply GFRP plates were measured. The maximum thickness difference measured within a 300 mm x 280 mm plate was 8.1% and 4.6% mm for the 8 plies thick CFRP and GFRP plates respectively. The standard deviation on the thickness of the plates as reported in Table I suggests that the manufacturing process developed produced laminates of consistent thickness and with only minor disparities within each plate.

F. Resin Burn-Off

A resin burn-off test according to ASTM D3171-15 was performed to measure the Fibre Volume Fraction (FVF) of the CFRP and GFRP samples. Small samples were extracted off various locations within each plate at the same time as specimens used in DCB and tensile tests and weighted using an Ohaus precision scale. They were placed in a furnace where the temperature was ramped up to 450°C in 90 minutes and kept at 480°C for 12 hours which is a temperature high enough

TABLE II
FVF MEASUREMENTS OF THE COMPOSITE PLATES

Material	Average FVF(%)	Standard Deviation (%)
Carbon Fibre	53.7	1.8
Glass Fibre	49.9	2.2

to ensure complete resin combustion but low enough to maintain the carbon fibres intact. FVF measurements were taken for a total of six CFRP and GFRP plates and are summarised in Table II. In order to reach a target fibre volume fraction of 50% and as both fabrics have roughly the same area weight, more powder needed to be placed between the carbon plies during manufacturing. This led to more bleed-out for the carbon laminates which explains the higher average FVF obtained. The standard deviations were of similar magnitude for both plates and was relatively low, showing that this manufacturing process is repeatable and reliable. This test was also used to obtain an estimation of the void content in the laminates which was found to be 0.1% for the CFRP and 1.6% for the GFRP. However, these results were rough estimates, especially for the glass fibre plates, as the fibre density was only known to one decimal point.

G. Microscopy

Small 20 mm by 15 mm samples were cut in the transverse fibre direction for both the carbon fibre and glass fibre samples. They were placed within an epoxy resin matrix, which was cured at room temperature for 24 hours, followed by 5 hours of post-cure at 50°C. The samples were then polished on an automatic polishing machine using sandpaper with increasing grit size (P400, P800 and P1200). To obtain a very smooth surface for optical micrographs, the samples were then polished using a diamond based dispersion with a 3 μm particle size. The laminates were then observed under a Zeiss optical microscope fitted with an AxioCam MRc 5 camera. The fibres and resin were observed up to 50X zoom as shown in Fig. 3. The black marks around some of the fibres are machining marks which were not successfully removed by the polishing process. However, observations of both the CFRP and GFRP plates show that there were no visible macro voids in the samples studied. Indeed, these would appear as dark circular spots on Fig. 3 [19]. Although a more precise imaging method such as SEM or CT-scan would be required to confirm the exact void content, the results from the optical micrographs as well as from the resin burn-off both seem suggest that the void content is very low for these laminates.

IV. RESULTS AND DISCUSSION

H. Tensile Testing

The results of the tensile tests are summarised in Table III. The results for the glass fibre reinforced powder epoxy showed only minor variability between coupons with a Coefficient of Variation (COV) of 8.4%
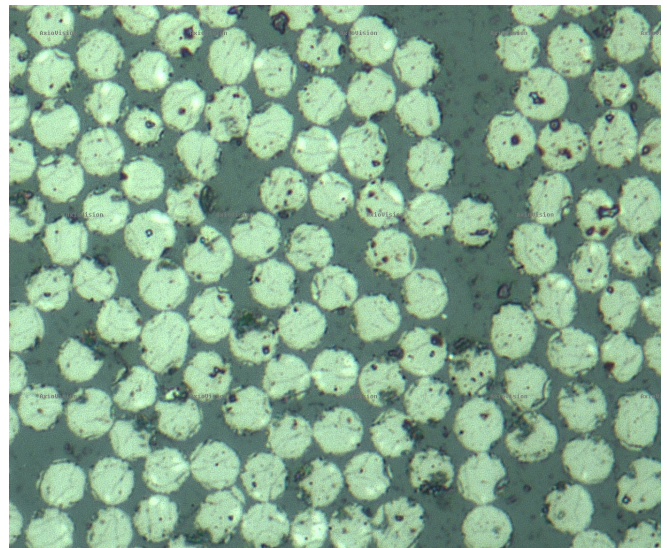

Fig. 3. Optical Microscope Image of CFRP Sample at 50X Zoom.

for the shear modulus but of only 3.7% for the longitudinal tensile strength. On the other hand, the standard deviations obtained for the carbon samples were much higher with COV of 13.7% for the longitudinal tensile strength and 15.6% for the shear modulus. However, the standard deviations were much lower for the 90° specimens, where the failure behaviour was matrix dominated.

Inspection of the failed composites suggested that there was a problem with fibre alignment in the CFRP plates. As there are very few off-axis fibres and stitching, the fibre tows for the carbon fibre fabrics were very loose and hence, the plates were hard to manufacture without distorting some of fibre bundles. Following analysis of these results, greater care needs to be taken during the plate layup to ensure that fibres were kept straight and further samples will be tested again in an attempt to obtain more consistent data. As is often the case in composites manufacturing, the properties of the final laminate are partly dependent on the skill of the individual. Still, it is worth noting that similar values for the strength and stiffness of Zoltek PX35 50K with a 50% fibre volume fraction can be found in the literature [20], albeit with a different fabric.

A material datasheet from Zoltek [21] which lists the longitudinal mechanical properties of UD Zoltek PX35 unidirectional fabrics manufactured using standard epoxy resin with an FVF of 55% was used to evaluate the performance of powder epoxy compared to standard epoxy resin. As the datasheet did not specify the exact composition of the resin, fabric and manufacturing method, it was difficult to perform a rigorous comparison between the two epoxy systems. However, the obtained longitudinal strength and stifness of 1492 MPa and 123 GPa respectively were higher than the 1400 MPa and 119 GPa listed by the manufacturer. Icten et al. [22] characterised the mechanical properties of an e-glass unidirectional composite with CY336 epoxy resin which was manufactured in a hot press to an FVF of 65%. They reported a longitudinal strength and stifness of 783 MPa and 40.5 GPa respectively which is

TABLE III
TENSILE TEST RESULTS

Property	GFRP			CFRP		
	Result	Standard Deviation	COV	Result	Standard Deviation	COV
Longitudinal Modulus E_1 (GPa)	39.4	0.65	1.6%	123.0	6.7	5.4%
Longitudinal Strength σ_1 (MPa)	993	37	3.7%	1492	205	13.7%
Transverse Modulus E_2 (GPa)	13.7	0.77	5.6%	8.47	0.37	4.4%
Transverse Strength σ_2 (MPa)	98.0	5.3	5.4%	31.5	1.9	6.0%
Shear Modulus G_{12} (GPa)	3.91	0.33	8.4%	4.30	0.67	15.6%
Shear Strength τ_{12}	71.6	2.6	3.6%	64.2	1.2	1.9%
Poisson's Ratio v_{12}	0.29	0.093	32.1%	0.36	0.086	23.9%

a lower strength than the 993 MPa obtained as part of this study but a marginally higher stiffness despite a substantially higher fibre volume fraction. The reported transverse modulus of 13.96 GPa was very similar to the 13.7 GPa listed in Table III. Similarly, Gopalakrishnan et al. [23] evaluated the mechanical properties of 300 gsm YD e-glass with LY556 epoxy resin manufactured by wet layup to an FVF of 55%. They found a lower longitudinal strength and stifness than that obained for the powder epoxy glass fibre composite with 821 MPa and 33 GPa respectively. However, the datasheet provided by SAERTEX [18] does not provide detailed information on the e-glass fibre properties and therefore the fibres might have also played a role in the better mechanical properties obtained for the powder epoxy laminate. The insufficient details released on the datasheets means caution needs to be taken before asserting that powder epoxy composites perform better than conventional ones although it can be said that the use of this novel resin system does not seem to lead to a degradation of in-plane mechanical properties.

The results for the GFRP specimens showed very good consistency as revealed by the small standard deviations. This was encouraging as it shows that the manufacturing process produced reliable and repeatable parts and that would lead to a reduction in the safety factor required when designing composite structures. As expected, the transverse modulus and strength were significantly higher for the GFRP than for the CFRP specimens. This was linked to the presence of about 9% transverse fibres as opposed to the carbon samples which possess only 2.7% off-axis fibres, which were in the $\pm60°$ directions.

I. Mode I Fracture Toughness

The mode I interlaminar fracture toughness was determined experimentally for the CFRP samples by conducting DCB tests. During this test, the crack opening displacement at the load blocks, the force and the crack extension were all measured. The results, which are displayed in Fig. 4, showed that the shapes of the force-displacement curves were very similar for all five samples with a linear response up until about 110N followed by a small deviation from linearity until the maximum force was reached at around 135N. This is the behaviour typically observed in literature [24] and is linked to the initiation of damage in the process
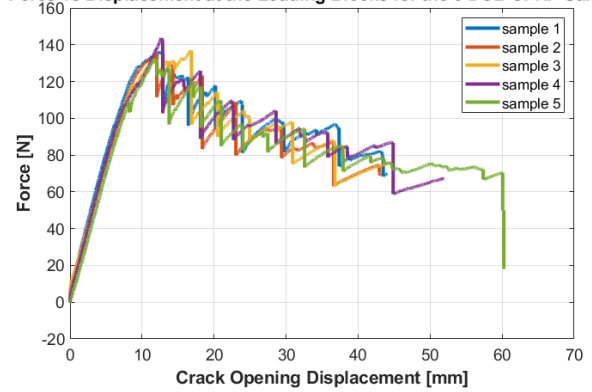

Fig. 4. Force vs Displacement at the Loading Blocks for the CFRP samples.

zone ahead of the crack tip in the form of resin micro cracking [25]. Following the peak load, there was a sudden decrease in the force as the crack started to visibly extend followed by a gradual decrease in the load with an increase of the crack propagation. However, the downward trend of the load was not smooth and in fact, the curve exhibited a stick-slip behaviour, which is characterised by alternating periods of slow crack growth as the load increases followed by a sudden drop of load and increase in crack length. This phenomenon might be caused by local variations in the material properties, such as the presence of resin rich areas at the interface. In this case however, an image captured during the DCB test shown in Fig. 5 revealed that fibre bridging occurred. The $\pm60°$ fibres in the UD carbon fabric were pulled from the layers surrounding the crack and led to an increased resistance to crack propagation, and consequently increased loads. However, these fibres eventually snapped leading to an instant reduction in the fracture toughness and increase in the crack extension.

The interlaminar fracture toughness was calculated from the DCB test results using the Modified Beam Theory (MBT). The normal beam theory with which G_{IC} is calculated assumes that the delamination end is fully clamped. However, as evidenced in Fig. 5, there is some rotation leading to an overestimation of the G_{IC}. This can be corrected by considering the crack to be slightly longer than measured. The G_{IC} was then measured as follows:
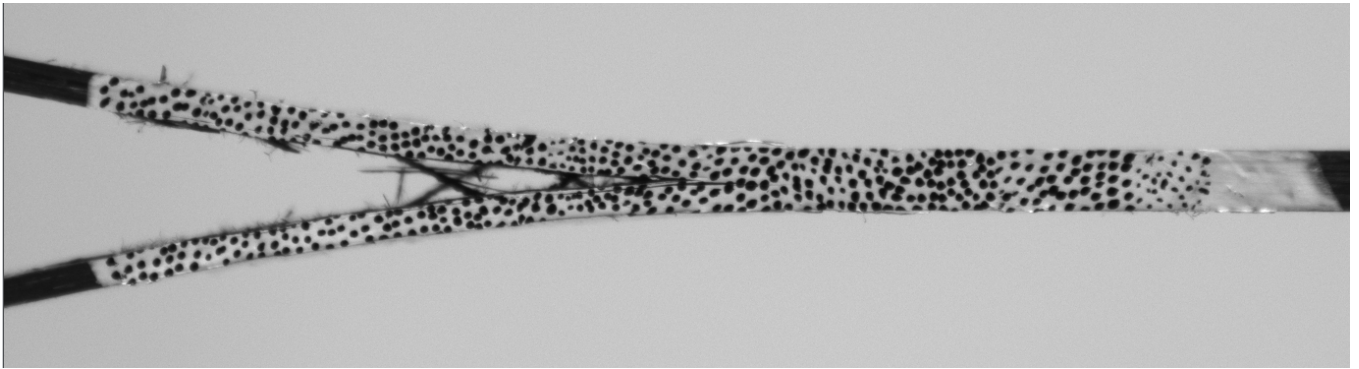
Fig. 5. CFRP Sample during DCB Test Exhibiting Fibre Bridging.

$$G_{IC} = \frac{3P\delta}{2b(a + |\Delta|)} \qquad (2)$$

Where P is the force applied on the loading blocks, δ is the displacement at the load point, b is the width of the sample, a is the delamination length and Δ is a correction factor which can be determined by plotting the linear best fit of the cube root of the compliance against the crack length and calculating the root of this function.

The evolution of G_{IC} as a function of crack length for a representative sample is shown in Fig. 6 and there is a good agreement between the samples. It is important to note that because of the stick slip behaviour, the fracture toughness was not constant throughout the test and did not converge to a stable value. Instead, it was fluctuating between roughly 1500 and 2400 J/m^2. The G_{IC} was taken as the average of all the values measured from the first moment the crack was visibly extended up until the crack extension data was lost by the camera. The average mode I interlaminar fracture toughness was measured at 1900 J/m^2 with a standard deviation between specimens of only 57 J/m^2 which corresponds to a COV of 3.0%.

Some reported values for the fracture toughness of various carbon fibre reinforced epoxy prepreg composites are summarised in Table IV. It shows that the powder epoxy composite studied in this work has more than double the G_{IC} of typical carbon/epoxy prepregs, which indicates that this composite system is a good material choice, especially in regions of high stress such as tidal turbine blade root sections where delamination may occur.

TABLE IV

MODE I INTERLAMINAR FRACTURE TOUGHNESS FOR CARBON/EPOXY COMPOSITES

Material	Average G_{IC} (J/m^2)
T300/Toughened Epoxy (HS 160 REM) Prepreg	900 [24]
High Strength Carbon/Epoxy Prepreg	850 [15]
T300/934 prepreg	640 [26]
Zoltek Panex 35/ Powder Epoxy	1900 ±57

V. CONCLUSION AND FUTURE WORK

A manufacturing process was developed using a frame to manufacture 300 mm x 280 mm carbon fibre and glass fibre reinforced powder epoxy plates. An investigation into the quality of the laminates demonstrated low thickness variations between different laminates (2% maximum). Also, the disparity in the thickness within each plate was relatively small. The fibre volume fraction was shown to be close to the target 50% for GFRP and slightly higher for CFRP with a standard deviation of around 2%. Finally, no macro voids were visible upon observation under an optical microscope. These results highlighted the reliability of this new process which allows the production of consistent plates.

The mechanical properties of the CFRP and GFRP were characterised and the glass fibre laminates exhibited very low scatter. The carbon fibre samples on the other hand showed greater variability in the longitudinal tensile strength. A low percentage of off-axis fibres and stitching resulted in the fibre bundles within the carbon fibre fabric being succeptible to warping. This made it difficult to ensure uniform fibre alignement during manufacturing. This will be investigated in future work where the fibre straightness will be monitored carefully during the manufacturing process. It was also found that the in-plane mechanical properties of the powder epoxy composites were comparable and in some cases marginally better than composites manufactured with conventional epoxy resins.

The mode I interlaminar fracture toughness of the CFRP laminates was investigated by carrying out DCB tests and an average G_{IC} of 1900 J/m^2 was measured. This value is significantly higher than the values reported in the literature for carbon/epoxy prepregs with more than double the G_{IC} value. This makes this system very promising for potential applications in composite structures where high stresses exacerbate the risk of delamination such as in the root section of a tidal turbine blade. The force-displacement curves and the behaviour of the specimens throughout the tests were very similar with a coefficient of variation in the average fracture toughness found to be only 3.0%.

This work was an initial step in a wider study on the fracture properties of novel powder epoxy composites. Future work will include conducting DCB tests on
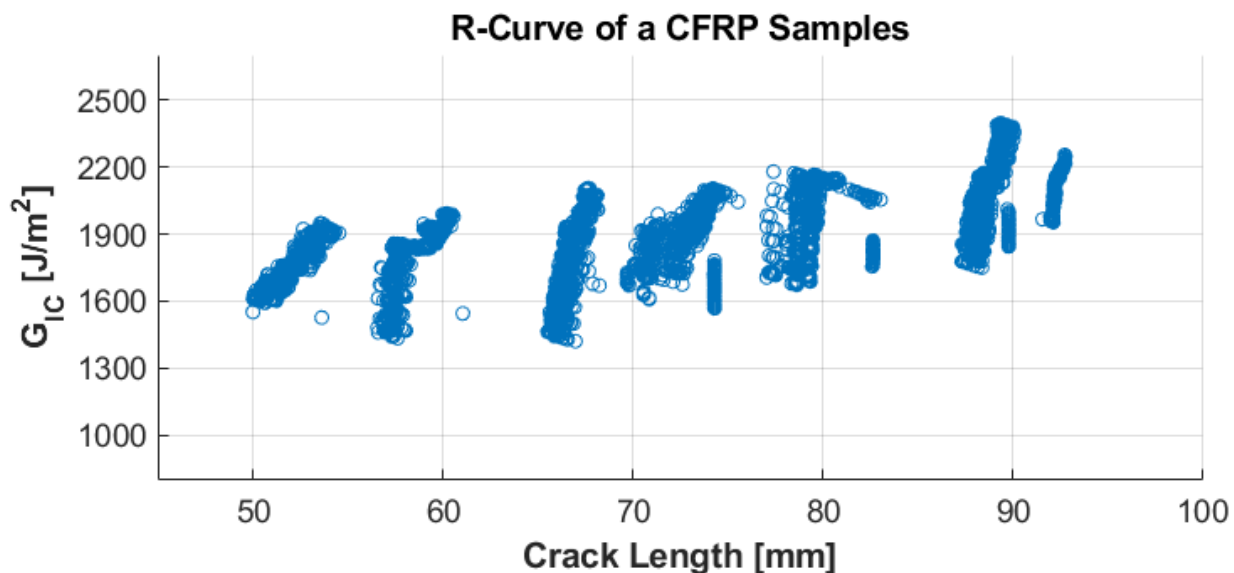
Fig. 6.   R-Curve of a CFRP Sample.

GFRP laminates. This will be followed by immersion of GFRP and CFRP samples in seawater until saturation so that a DCB test can be performed on the wet composites to understand and quantify the effect of water aging on the mode I fracture toughness. Finally, in most real composite structures, delamination does not occur in either mode I or mode II but rather a mix of the two. Therefore, the full interlaminar fracture toughness properties of the CFRP and GFRP will be investigated by carrying out Mixed Mode Bending (MMB) test.

REFERENCES

[1] E. Segura, R. Morales, J. A. Somolinos, and A. López, "Techno-economic challenges of tidal energy conversion systems: Current status and trends," *Renewable Sustainable Energy Review*, vol. 77, pp. 536–550, 2017.

[2] C. EU-OEA, "Oceans of energy: European Ocean Energy Roadmap 20102050," *European Ocean Energy Association*, 2010.

[3] S. B. Elghali, M. Benbouzid, and J. Charpentier, "Modelling and control of a marine current turbine-driven doubly fed induction generator," *IET Renewable Power Generation*, vol. 4, p. 111, 2010.

[4] S. Giorgi and J. V. Ringwood, "Can tidal current energy provide base load?" *Energies*, vol. 6, pp. 2840–2858, 2013.

[5] S. Astariz, A. Vazquez, and G. Iglesias, "Can tidal current energy provide base load?" *Journal of Renewable and Sustainable Energy*, vol. 7, no. 5, 2015.

[6] L. E. Myers and A. S. Bahaj, "An experimental investigation simulating flow effects in first generation marine current energy converter arrays ," *Renewable Energy*, vol. 37, pp. 28–36, 2012.

[7] T. Flanagan, J. Maguire, C. M. Ó Brádaigh, P. Mayorga, and A. Doyle, "Smart Affordable Composite Blades for Tidal Energy ," *Proceedings of the 11th European Wave and Tidal Energy Conference*, pp. 1–8, 2015.

[8] R. Evans, R. Mcadam, M. Royle, and L. Mcewen, "Optimum geometry for axial flow free stream tidal turbine blades ," *European Wave and Tidal Energy Conference 2013*, 2013.

[9] D. M. Grogan, S. B. Leen, C. R. Kennedy, and C. M. Ó Brádaigh, "Design of composite tidal turbine blades," *Renewable Energy*, vol. 57, pp. 151–162, 2013.

[10] L. Sorrentino, W. Polini, and C. Bellini, "To design the cure process of thick composite parts: experimental and numerical results," *Advanced Composite Materials*, vol. 23, pp. 225–238, 2014.

[11] C. M. O Bradaigh, A. Doyle, D. Doyle, and P. J. Feerick, "Electrically-Heated Ceramic Composite Tooling for Out-of-Autoclave Manufacturing of Large Composite Structures," *SAMPE Journal*, vol. 47, no. 4, pp. 6–14, 2011.

[12] J. M. Maguire, K. Nayak, and C. M. Ó Brádaigh, "Characterisation of epoxy powders for processing thick-section composite structures," *Materials & Design*, vol. 139, pp. 112–121, 2018.

[13] N. McEwen, R. Evans, and M. Meunier, "Cost-effective tidal turbine blades," *4th International Conference on Ocean Energy (ICOE2012)*, 2012.

[14] E. M. Fagan, C. R. Kennedy, S. B. Leen, and J. Goggins, "Damage mechanics based design methodology for tidal current turbine composite blades," *Renewable Energy*, vol. 97, pp. 358–372, 2016.

[15] P. Harper and S. Hallett, "Advanced numerical modelling techniques for the structural design of composite tidal turbine blades," *Ocean Engineering*, vol. 96, pp. 358–372, 2015.

[16] S. P. Blake, K. A. Berube, and R. A. Lopez-Anido, "Interlaminar fracture toughness of woven E-glass fabric composites," *Journal of Composite Materials*, vol. 46, pp. 1583–1592, 2012.

[17] SAERTEX®, "U-C-603g/m^2-1230mm Technical Datasheet," 2019. [Online]. Available: https://www.saertex.com/en/products/datasheet-carbone

[18] SAERTEX®, "U-E-591g/m^2-1200mm Technical Datasheet," 2019. [Online]. Available: https://www.saertex.com/en/products/datasheet-glass

[19] Y. Hamidi, L. Aktas, and M. Altan, "Formation of Microscopic Voids in Resin Transfer Molded Composites," *ASME Journal of Engineering Materials and Technology*, vol. 126, pp. 420–426, 2004.

[20] J. Murray, E. Pappa, D. Mamalis, G. Breathnach, A. Doyle, T. Flanagan, S. Di Noi, and C. M. Ó Brádaigh, "Characterisation of Carbon Fibre Reinforced Powder Epoxy Composites for Wind Energy Blades," *18th European Conference on Composite Materials ECCM18*, vol. 46, 2012.

[21] Z. Corporation, "Zoltek™ PX35 Uni-Directional Fabrics Technical Datasheet," 2018. [Online]. Available: http://zoltek.com/wp-content/uploads/2018/06/TDS_PX35_Uni-Directional_Fabric.pdf

[22] B. Icten, C. Atas, M. Aktas, and R. Karakuzu, "Low temperature effect on impact response of quasi-isotropic glass/epoxy laminated plates," *Composite Structures*, vol. 91, no. 3, pp. 318 – 323, 2009.

[23] M. Gopalakrishnan, S. Muthu, R. Subramanian, R. Santhanakrishnan, and L. M. Karthigeyan, "Tensile properties study of e-glass/epoxy laminate and /4 quasi-isotropic e-glass/epoxy laminate," *Polymers and Polymer Composites*, vol. 24, no. 6, pp. 429–446, 2016.

[24] A. B. De Morais and A. B. Pereira, "Application of the effective crack method to mode I and mode II interlaminar fracture of carbon/epoxy unidirectional laminates," *Composites Part A: Applied Science and Manufacturing*, vol. 38, pp. 785–794, 2007.

[25] A. B. De Morais and M. F. S. F. De Moura, "Evaluation of initiation criteria used in interlaminar fracture tests," *Engineering Fracture Mechanics*, vol. 73, pp. 2264–2276, 2006.

[26] L. Ye, "Evaluation of Mode-I interlaminar fracture toughness for fiber-reinforced composite materials," *Composites Science and Technology*, vol. 43, pp. 49–54, 1992.